Locked and Unlocked Smooth Embeddings of Surfaces

David Eppstein
Department of Computer Science, University of California, Irvine

Abstract

We study the continuous motion of smooth isometric embeddings of a planar surface in three-dimensional Euclidean space, and two related discrete analogues of these embeddings: polygonal embeddings and flat foldings without interior vertices, under continuous changes of the embedding or folding respectively. For each of these three models of continuous motion, we show that every star-shaped or spiral-shaped domain is unlocked: a continuous motion unfolds it to a flat embedding. Here, a domain is spiral-shaped if it can be reduced to a point by a continuous family of similarities whose images remain within the domain; we prove that polygons with this property can be recognized in linear time. However, we provide an example of a disk with two holes that has locked embeddings: its embeddings are topologically equivalent to a flat embedding but cannot reach a flat embedding by continuous motion.

Keywords and phrases geometric reconfiguration, developable surface, flat folding, spiral-shaped domain

Digital Object Identifier 10.57717/cgt.v2i2.28

Funding Research supported in part by NSF grant CCF-2212129.

Acknowledgements This work was inspired by discussions at the 3rd Virtual Workshop on Computational Geometry, held in March 2022, for which we thank the organizers and participants. A preliminary version of this work appeared at the 34th Canadian Conference on Computational Geometry (CCCG 2022).

1 Introduction

Much research in computational geometry has examined the ability to deform a shape while preserving its geometric structure. A classical example is the "carpenter's rule", a polygonal chain whose allowed motions may continuously change any vertex angle, but may not change the lengths of its segments or introduce self-crossings between them. Any carpenter's rule in two dimensions may be continuously unfolded so that it lies flat, on a straight line [27, 9, 22]. However, carpenter's rules in three dimensions can have *locked* configurations, unable to reach a straightened configuration even though there is no topological obstacle to their reconfiguration [18, 4, 5, 12, 3, 8]. Other similar geometric reconfiguration problems include bloomings, continuous and collision-free unfoldings from polyhedra to flat nets that preserve the shape of each face [26, 6, 20, 10, 31, 16], and the continuous rigid motions of single-vertex origami patterns [28, 21, 1]. Demaine, Devadoss, Mitchell, and O'Rourke studied "folded states" of simple planar polygons in $\mathbb{R}^3$, which they defined in terms of a surface-distance-preserving mapping to $\mathbb{R}^3$ together with a consistent "local stacking order" at parts of the polygon that are mapped onto each other. As they showed, any folded state can be continuously transformed to any other folded state: the configuration space of these states is connected [13, 11]. In this work we study the reconfigurability of three natural restricted forms of these folded states:

- Smooth isometric embeddings into $\mathbb{R}^3$, where the embedded surface is doubly differentiable (having a tangent plane everywhere) without self-contact. Here, "isometric" means that distances, as measured by curves along the embedded surface, must remain unchanged,

but the embedding is otherwise free to vary continuously.

- Polygonal (piecewise linear) isometric embeddings into $\mathbb{R}^3$ without interior vertices. Here, the points where the mapping is not locally linear must extend across the surface in a line segment from boundary to boundary; we call this a *fold line*. We require the embedding to have finitely many connected linear pieces, and no self-contact. The folds or bend lines are not fixed in their positions; they may "roll" along the surface, rotate in place, or appear and disappear as dihedral angles reach π.
- Planar folded states (flat foldings) without interior vertices. We again require that the mapping be piecewise linear with finitely many pieces and that the fold lines extend from boundary to boundary across the surface, allowing them to roll or rotate as the mapping changes continuously. However, in this case, the piecewise linear mapping is from $\mathbb{R}^3$ to $\mathbb{R}^2$, so self-contact is unavoidable.

The reconfigurability of these embeddings is complicated by a certain form of rigidity that they share, which is not present in less-restricted embeddings. Whenever a flat surface is smoothly embedded into $\mathbb{R}^3$, each point where the embedding is curved must belong to a "bend line" on the surface, a line segment that extends from boundary to boundary on the surface, and is embedded as a line segment in $\mathbb{R}^3$ [15]. The system of bend lines, found in this way, can hold the surface rigid in one of its two dimensions, while allowing it to flex in the other dimensions. A familiar example can be found in a slice of pizza, held at the crust. If one attempts to hold the pizza flat, its tip will droop, but bending the slice lengthwise will extend rigid bend lines through the slice, preventing drooping [30]. Similarly, a large sheet of paper such as a loose poster can be very flexible, but a poster rolled into a tight cylinder becomes quite rigid: the cylinder cannot bend without crumpling (breaking the smoothness of its embedding). Our restriction against interior vertices of polygonal embeddings and flat foldings again causes fold lines to continue in a straight line from boundary to boundary of a given shape, providing a combinatorial model of the same phenomenon. We have studied flat foldings with this restriction (but not their reconfiguration) in previous work [14].

These models of folded states are closely related to each other. Any smoothly embedded developable surface[1] can be approximated arbitrarily closely by a polygonal surface without interior vertices (but with slightly different intrinsic geometry), obtained by using a subset of the bend lines of the smooth surface as fold lines of the polygonal surface, and adding intermediate fold lines between consecutive pairs of chosen bend lines that are smooth in space. In the other direction, any polygonal embedded surface without interior vertices can be approximated arbitrarily closely by a smooth surface, obtained by cutting away the surface close to any vertex where two or more fold lines meet and then approximating each fold by a small-radius cylindrical surface. The same approximation method, replacing folds by cylinders, also works for flat foldings with acyclic above-below relations, after lifting the overlapping pieces of the flat-folded surfaces to closely-spaced parallel planes. This method of lifting flat-folded surfaces to parallel planes and replacing folds by cylinders was already used in 1930 by Michael Sadowsky to prove that a Möbius strip, formed by twisting and joining the ends of a flat rectangle, has a smooth embedding whenever the aspect ratio of the rectangle exceeds $\sqrt{3}$ [17].

[1] A *developable surface* is a doubly-differentiable surface with everywhere-zero Gaussian curvature. Smooth isometric embeddings of a flat subset of the plane are automatically developable, but not vice versa; for instance, removing the apex from a cone produces a developable surface that is not an isometric embedding of a plane surface.

Our folded states are special cases of the ones previously considered by Demaine et al. [13, 11], and we retain their notion of a continuous motion as a mapping from the closed unit interval $[0, 1]$ to folded states that is continuous under the sup-norm of the distances of mapped points and (for flat foldings) consistent with respect to the local stacking order. The initial configuration of a motion is the mapping for the parameter value 0, and the final configuration is the mapping for the parameter value 1. For all three of our models of folded states, we prove the following new results:

- If a compact subset of the plane can be reduced to a point by a continuous shrinking motion (a continuous family of similarity transformations whose images all remain within the shape) then it has a connected space of folded states: every smoothly embedded or folded state can be continuously unfolded to a flat state (one that lies within a single plane, with no self-overlaps). The sets to which this result applies are topological disks and include all star-shaped domains.
- There exist subsets of the plane, topologically equivalent to a disk with two holes, that can be locked: they have embeddings that are topologically equivalent (ambient isotopic) to their embedding as a subset of a plane, but from which continuous deformations within the same folding model cannot reach this flat state.

As an auxiliary result in an appendix, we prove that the polygons that have a continuous shrinking motion can be recognized in linear time.

2 Shapes that can shrink into themselves

A *star-shaped* polygon, or more generally a star-shaped domain, is a subset S of the plane such that, with an appropriate choice of one point of the plane to be the origin, every scaled copy pS for $p \in [0, 1]$ is a subset of S itself. These are widely studied in computational geometry, and can be recognized in linear time [19]. However, these are not the only shapes that have a continuous shrinking motion of scaled copies of the shape into themselves. Figure 1 depicts a different type of continuous shrinking motion, in which the shape spirals inwards while shrinking. Such a motion can be described by coordinatizing the plane by complex numbers, again for an appropriately chosen origin (the center of the spiral motion), choosing a complex number q of absolute value less than one, and considering the family of scaled copies $q^p S$ for $p \in [0, \infty)$. The linear shrinking motion of star-shaped domains is a special case of this type of motion in which q is a real number in the interval $(0, 1)$.

Not every continuous shrinking motion is of this form. Once a shape has shrunk to a small fraction of its original size, there is considerable freedom in how it may continue to move and shrink without passing outside its original area. However, near the start of the motion (in a technical sense, as a limiting case of the part of the motion that shrinks the shape from scale 1 to $1 - \varepsilon$, in the limit as $\varepsilon \to 0$), the motion must approximate this type of spiral shrinking motion. As a consequence, there must exist a center of this limiting motion, and a complex scaling factor q, such that the motion defined by this center and by q, in its initial moments, causes the shape to shrink within itself. If this is the case, then at all subsequent times, the same spiral shrinking motion will remain within the shrunken copies of the shape immediately before them in the motion, and therefore within the original shape as well. In this sense, the inward-spiraling shrinking motions defined in this way are completely general: if a shape has any continuous shrinking motion, it has an inward-spiraling shrinking motion. Following Aharonov et al. [2], we call a compact set S that has a continuous shrinking motion of this type a *spiral-shaped domain*. In Appendix A, answering a question posed in the conference

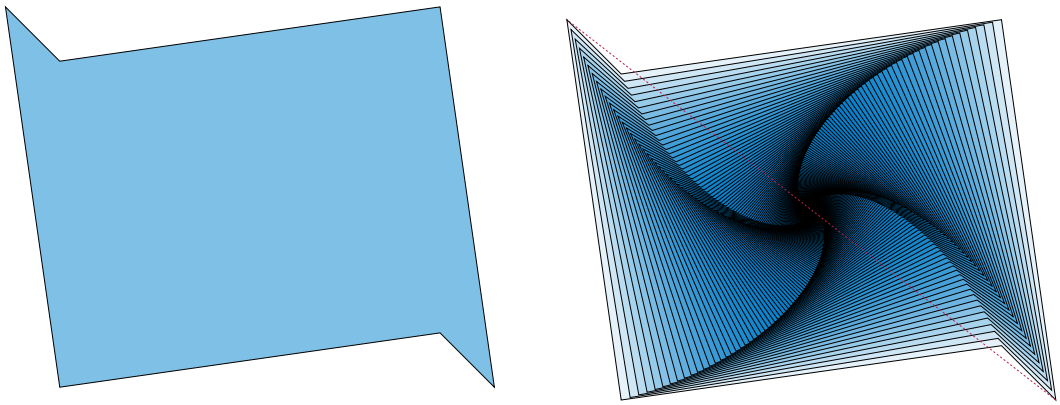

Figure 1 A polygon (left) with a continuous shrinking motion (right). The red dashed line connecting two opposite corners through the center of the motion demonstrates that this polygon is not star-shaped: no point on one side of the red dashed line can see into the corner on the other side of the line. As the polygon shrinks, these corners trace out logarithmic spirals; the angle made by these spirals with the red dashed line is the *polar tangential angle* of its spiral.

version of this paper, we prove that testing whether a polygon forms a spiral-shaped domain can be done in linear time, by applying algorithms for LP-type optimization problems.

The main results of this section are that every spiral-shaped domain S has a connected space of smooth embeddings, a connected space of polygonal embeddings without interior vertices, and a connected space of flat-foldings without interior vertices. Equivalently, every embedding of each type can be continuously unfolded. The simplest case concerns smooth embeddings.

▶ **Theorem 1.** *Every smooth embedding of a spiral-shaped domain has a continuous motion, through smooth embeddings, to a flat embedding.*

Proof. Let S be the given spiral-shaped domain, and $f : S \to \mathbb{R}^3$ be its smooth embedding. Parameterize an inward-spiraling shrinking motion of S as $s_i : S \to S$ where $i \in (0, 1]$, s_1 is the identity, and each s_i scales S by a factor of i, converging as $i \to 0$ to a single central point of the motion (which may or may not be on the boundary of S).

Our proof converts this parameterized family of scalings to a parameterized family of smooth embeddings of S at a single scale, by composing s_i, f, and a function that expands $\mathbb{R}^3$ by a factor of $1/i$ to restore the original size of S. The obvious expansion function $\mathbb{R}^3$ by $(x, y, z) \mapsto (x/i, y/i, z/i)$ does not work, because of the following issues:

- Composing s_i, f, and an expansion by $1/i$ does provide a continuous motion of smooth embeddings on the half-open interval $(0, 1]$, whose maximum curvature tends towards zero as the parameter goes to zero.[2] However, we need a continuous motion on the closed interval $[0, 1]$ for which the limiting embedding at parameter value zero exists and is completely flat.
- When the origin of $\mathbb{R}^3$ does not belong to all of the rescaled and smoothly embedded copies of S, the composition with $\mathbb{R}^3$ by $(x, y, z) \mapsto (x/i, y/i, z/i)$, as $i \to 0$, will produce

[2] The *maximum curvature* is the maximum of the *normal curvatures*, the curvatures that can be obtained at some point p of the surface by intersecting the surface with a plane containing p and its normal vector, and using the curvature at p of the resulting plane curve. Thus, when the maximum curvature tends towards zero, so do all normal curvatures. This is stronger than merely requiring that the Gaussian curvature tend towards zero, which is true for all developable surfaces.

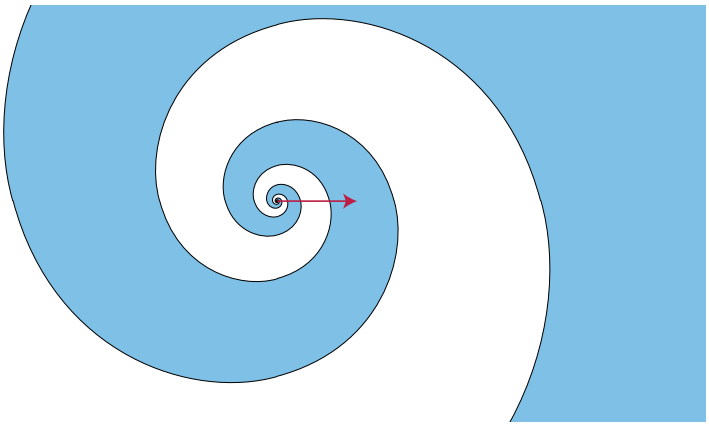

Figure 2 A spiral-shaped domain between two logarithmic spirals. In any continuous shrinking motion, this domain retains the same spiral form near the center p of the spiral, preventing later stages of the shrinking motion from being shortcut to a linear motion. The red arrow depicts a vector at p, whose image under any smooth embedding of f (that is, the vector tangent to the embedded surface at $f(p)$ with the same direction and length) can be used as the reference vector in the proof of Theorem 1.

smooth embeddings of S whose distance from the origin is inversely proportional to i, preventing them from having a limit. We can prevent this by choosing coordinates for $\mathbb{R}^3$ that have as their origin $f(p)$, where p is the limit point of the inward-spiraling shrinking motion on S. In this way, the composition of s_i, f, and an expansion by $1/i$ will act as the identity on this point, and more strongly will preserve the tangent plane of the surface at that point.

- This still does not complete the proof, because a spiral inward-shrinking motion of the domain, composed with f and $(x, y, z) \mapsto (x/i, y/i, z/i)$, will cause the embeddings to rotate at increasing speed as $i \to 0$, preventing the continuous motion from having a flat limiting surface at $i = 0$. For the polygonal domain of Figure 1, this problem can be circumvented by switching from the spiral inward-shrinking motion to a linear scaling transformation in S, once the scaled copies of S become small enough that this linear scaling stays entirely within S. However, for some other shapes, such as the domain between two logarithmic spirals depicted in Figure 2, switching to linear scaling is never possible. Instead, we address this third issue by choosing a reference vector tangent to S at $f(p)$. We compose s_i, f, an expansion by $1/i$, and a rotation of $\mathbb{R}^3$ (with axis perpendicular to the tangent plane at $f(p)$) that restores this vector to its original direction.

Let f_i denote the resulting composition of s_i, f, an expansion of $\mathbb{R}^3$ with a careful choice of origin, and a rotation that restores the original directions of vectors in the tangent plane to the embedded surface. Then f_i, for values of i in the half-open interval $(0, 1]$, describes a continuous motion with $f_1 = f$ as one endpoint of the motion.

Recall that the maximum curvature of a surface is the maximum of the normal curvatures at any of its points, and that the normal curvature is defined as the curvature of a plane curve in a tangent plane, that is, the inverse of the radius of an osculating circle to the curve in that plane. To calculate the behavior of this maximum curvature in the limit, we combine the following observations.

- Because $f(S)$ is smooth and compact, its normal curvatures have a maximum, κ.
- Taking a subset $f(s_i(S))$ of the surface $f(S)$ does not change the normal curvatures at

the points of the subset, and only restricts the set over which we are taking a maximum, so its maximum curvature is still at most κ.
- Scaling the surface by a factor of $1/i$ scales each osculating circle in each normal plane by the same factor. Therefore it scales each normal curvature, and the maximum curvature defined from them, by i. As a result, the $1/i$-scaled copy of $f(s_i(S))$ will have maximum curvature at most $i\kappa$.
- Rotating to produce $f_i(S)$ does not change the curvature.

Letting i go to zero in the limit, this bound on the maximum curvature of $f_i(S)$ also goes to zero in the limit.

For each point $q \in S$, $f_i(q)$ can be obtained by the exponential map: follow a curve on $f_i(S)$ of length $|p - q|$, starting from p, in the direction given by the image of the tangent vector $q - p$. This length and direction are invariant through the motion, and as $i \to 0$ the curvature of this path approaches zero. Therefore, f_i converges pointwise to a flat embedding $f_0(S)$, obtained by the exponential map on the tangent plane of $f(S)$ at p. Appending f_0 to our continuous sequence of smooth embeddings f_i for $i \in (0, 1]$ gives us a continuous sequence on $i \in [0, 1]$, flat at $i = 0$ and equal to our starting embedding at $i = 1$, which therefore shows that these two embeddings are reconfigurable to each other. ◀

This proof uses compactness to ensure that the surface has finite maximum curvature. Non-compact surfaces can have self-similar embeddings, smooth everywhere except the limit point, that are invariant under shrinking and re-expansion. For example, a shape like that of Figure 2 can be wrapped onto a cone as an embedding into $\mathbb{R}^3$ that is smooth everywhere except at the tip of the cone. Shrinking and rescaling fails to flatten this example, because the point of the cone always retains its pointy shape. At this point, the normal curvatures are infinite or undefined. On the other hand, omitting this one non-smooth point from the shape would produce an embedding that is smooth everywhere, but not compact. The result does not have finite maximum curvature; instead it has arbitrarily large normal curvatures close to the cone point.

For polygonal embeddings we handle the same issue of avoiding self-similar embeddings differently, using the requirement that these embeddings have finitely many connected linear pieces.

▶ **Theorem 2.** *Every polygonal embedding without interior vertices of a bounded spiral-shaped domain has a continuous motion, through polygonal embeddings without interior vertices, to a flat embedding.*

Proof. The same idea as above comes close to working: compose the inward-spiraling shrinking motion of the domain, the initial embedding f, an expansion of $\mathbb{R}^3$ centered at the limit point of the motion, and a rotation of $\mathbb{R}^3$ that cancels any spinning motion the inward-spiraling motion might have. However, the limit point p of the inward-spiraling shrinking motion might be a point on a fold line of the polygonal embedding, or worse, it might be a boundary point of S where multiple fold lines meet. In either of these cases, we call p a *folding point*. When p is a folding point, there is not a unique tangent plane of $f(S)$ at p, and when the same composition can be made to have a limit, this limit will be folded at p in the same way as it was in $f(p)$ rather than being flat.

To address these issues, when p is a folding point of the embedding $f(S)$, we choose one of the polygonal faces incident to p to determine the tangent plane containing the reference vector of the previous construction. Then as above we compose the inward-spiraling shrinking motion of the domain, the initial embedding f, an expansion of $\mathbb{R}^3$ centered at the limit point of the motion, and a rotation of $\mathbb{R}^3$ that cancels any spinning motion of this tangent

plane. The resulting composition defines a continuous motion over the half-open interval of parameter values $(0, 1]$, which can be extended with a well-defined limit at 0, a polygonal folded state that has the same fold lines and fold angles as $f(S)$ at p and is flat everywhere else.

We distinguish three cases:

- If p is not a folding point of the embedding $f(S)$, then the previous proof applies directly.
- If p belongs to a single fold line of the embedding $f(S)$, then we can concatenate two continuous motions. First we perform the motion from the previous proof that transforms $f(S)$ into a folded state that contains this fold line. Because this folded state has only one fold line, it cannot self-intersect, and forms a valid polygonal embedding. Next, we perform an additional continuous motion that linearly changes the angle of this fold from its initial value to π (unfolded into a flat angle). Again, none of the intermediate states of this second continuous motion can self-intersect.
- In the remaining case, p is a boundary point of S that belongs to multiple fold lines within S. In the limiting folded state, the only folds are on line segments containing p. Such a folded line segment containing p must also be present in the original embedding, in order for it to appear in the limiting folded state. If the shrinking component contained any amount of rotation, this line segment through p would sweep out a topological disk surrounding p, an impossibility for a point that belongs to multiple fold lines. Therefore, the inward-spiraling shrinking motion must actually be the linear shrinking motion of a star-shaped domain, with p in its kernel. The *link* of this folded state at p, the intersection of $f_0(S)$ with a small sphere centered at p, is a polygonal chain consisting of arcs of great circles. Because it remains invariant throughout the motion, it does not self-intersect. Any two distinct points of S at distance d from p lie on distinct points of a scaled copy of this link, on a sphere of radius d, and for this reason cannot coincide. Therefore, the folded state at f_0 is again a valid polygonal embedding.

  By known results on the spherical carpenter's rule problem, there exists a continuous motion of the link, as a polygonal chain of fixed-length great-circle arcs on the sphere, from its folded state to a completely flat state. This motion induces a continuous motion of f_0 to a flat-folded state [28]. Performing the continuous motion from $f(S)$ to $f_0(S)$, and then using this carpenter's rule solution on the resulting single-vertex surface, produces a combined continous motion from $f(S)$ to a flat state. ◀

To apply the same method to flat foldings without interior vertices, we cannot use the carpenter's rule problem. A polygonal chain with fixed edge lengths, restricted to lie in a one-dimensional space (a line) has no continuous freedom of motion: it has only a discrete set of embeddings, and cannot move between them. In the same way, a flat folding of a two-dimensional disk, constrained to stay flat and to keep its folds fixed within the disk, cannot move. Therefore, to obtain an analogue of Theorem 2 for continuous motions that remain within the class of flat foldings, we must allow the folds to "roll" across the disk. This will happen automatically for some folds, in the first part of Theorem 2 using a continuous shrinking motion, but that may leave us with a limiting folded state that still has one or more folds through the center point of the motion. To handle these remaining folds, while remaining in a flat-folded state, we use a one-dimensional version of Theorem 2:

▶ **Lemma 3.** *Let P be a line segment, folded flat by a piecewise-isometry $f : P \to \mathbb{R}$ with a finite number of fold points and a consistent above-below relation for points with the same image. Then there exists a continuous motion of flat foldings of P that transforms folding f into an unfolded state.*

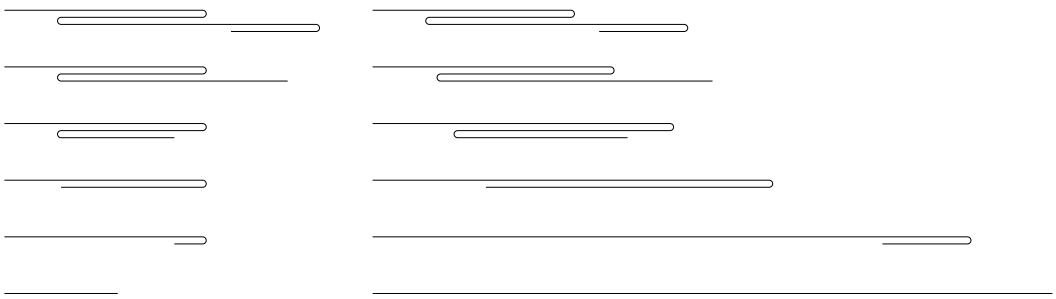

Figure 3 The unfolding process of Lemma 3, with p chosen as the left endpoint of the folded line segment. Left: The shorter folded line segments obtained by applying the same piecewise-isometry f to (top to bottom) the full line segment $P = [0, 1]$ and its scaled images $[0, i]$ for $i = 5/6, 2/3, 1/2, 1/3, 1/6$. Right: the folded line segments of the same length as $f(P)$ generated by expanding the left images by a factor of $1/i$.

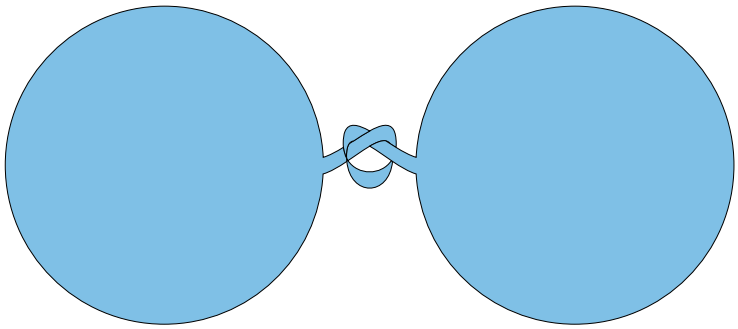

Figure 4 Two disks connected by a knotted band. This surface can be flattened by a continuous motion of smooth embeddings.

Proof. Choose any point p of P that is not a fold point, and form a continuous family of one-dimensional folded states of P, $f_i(P)$ for $i \in (0, 1]$, by scaling P by a factor of i centered at p, applying f, and scaling the result by a factor of $1/i$ centered at $f(p)$. When i becomes less than the distance from p to the nearest fold, the result will be an unfolding of P, so this provides a continuous transformation from f to an unfolding. ◀

Figure 3 demonstrates an example of this unfolding process, applied to the unit line segment $P = [0, 1]$, with $p = 0$, and with a piecewise-isometry f that maps P to a four-segment folded image.

▶ **Theorem 4.** *Every flat folding without interior vertices of a bounded spiral-shaped domain has a continuous unfolding motion through foldings of the same type.*

Proof. The proof follows the same outline as Theorem 2, combining shrinking and unshrinking to reach a folded state in which all folds pass through the center p of the spiral shrinking transformations. If the result has a single fold through p we roll this fold to the boundary of S rather than changing its fold angle. If p lies on the boundary of the domain and belongs to multiple fold lines, we apply Lemma 3 in place of the spherical carpenter's rule. ◀

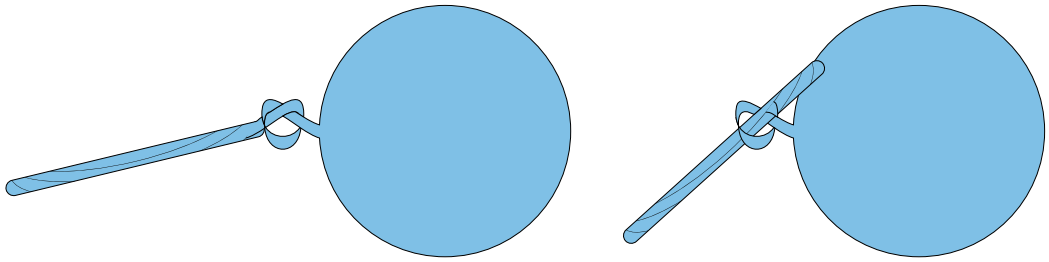

Figure 5 Intermediate states of unknotting the surface from Figure 4

3 The knotted dumbbell

In this section we briefly examine an example shown in Figure 4. We include it to demonstrate that the ability of bend lines to rotate in place can lead to unintuitive outcomes, highlighting the need for careful and rigorous reasoning about the reconfiguration of smooth surfaces. In this example, two large disks are connected by a short thin band. They are embedded into $\mathbb{R}^3$ with the disks spread flat and the band tied into an open overhand knot. By varying the dimensions of the example this knot can be made to be arbitrarily smaller than the disk diameter. If the disks could be crumpled, it would nevertheless be easy to untie and flatten this example, by crumpling the disks into small enough balls that they could be passed through the knot, and then uncrumpling. However, our model of smooth surface embeddings does not allow crumpling. In every smooth embedding, the center point of each disk lies in a flat subset of the disk with large diameter: either a diameter of the disk, or a triangular subset of the disk with the vertices of this triangle on the boundary of the disk.

Rolling up either disk around a diameter makes that diameter act like a rigid line segment. Rolling both disks in this way can produce an embedding that closely resembles the locked polygonal chain with long "knitting needles" at its ends from Figure 1 of Biedl et al. [4]. Although the rolled-up disks are thin enough to pass through the knotted band, they are too long and rigid, in this form, to do so. Embedding a disk so that it has a large flat triangular subset, instead of rolling it around a diameter, is even worse: in this case the flat center region is too large to pass through the knot. Intuitive reasoning of this form suggests that the embedding of the figure is locked, unable to be unfolded into a flat configuration. However, this surface is unlocked! It can be unfolded through the following sequence of transformations:

- Let D be a diameter of one of the two disks, touching the boundary of the disk at its attachment point p with the knotted band. Roll up the disk around D, starting at one of the points of the disk that is farthest from D, and leaving the semicircle opposite that point exposed on the outside of the roll.
- Poke p into the hole made by the knotted band, so that if the rolled-up disk around D were not rigid, it could pass through the hole and untie the knot (Figure 5, left). However, because D is made rigid by the bending of the embedding as it rolls around D, only the very end of diameter D near p can pass into the hole.
- Continuously spin the parallel family of bend lines on the rolled-up disk, so that it rolls up around a different diameter than D. Choose the direction of spin that causes p to travel along the exposed semicircle along the rolled-up disk. As it does so, this will allow more of the diameter of the rolled-up disk to poke through the hole in the knot (Figure 5,

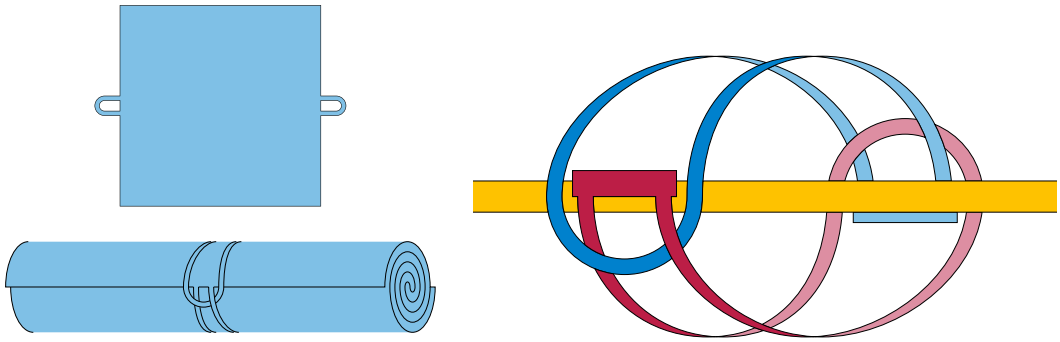

Figure 6 Left: A flat surface with two holes and a configuration that cannot be flattened. Intuitively, the two interlocked loops prevent the rolled center region from unrolling, the bend lines of the roll make it act like a rigid rod, and the length of this rod prevents the loops from being pulled around its ends. Right: Cutaway view of the two loops and centerline of the rolled-up part of the same surface, showing their topological equivalence to the Borromean rings.

right).

- When the bend lines have spun on the disk through an angle of π, causing p to reach the other end of the exposed semicircle, the rolled-up diameter will have traveled all of the way through the hole in the knot, which will become unknotted.
- Unroll the disk so that it lies flat with the rest of the surface.

Thus, although bend lines of a smoothly embedded surface are rigid, the underlying pattern of these lines on the surface can change continuously, complicating the search for a proof that a surface is locked.

4 The strapped rolled mat

Figure 6 depicts a smoothly-embedded unit square with two small loops on midpoints of opposite sides, wrapped into a spiral roll with the loops interlocked. The cutaway view on the right of the figure shows how the loops interlock. This rolled-up and interlocked surface is topologically equivalent (ambient isotopic) to a flattened surface. As can be seen in the cutaway view, the interlocking pattern is that of the Borromean rings, three unknotted loops in space that cannot be separated from each other, in which any two of the loops become unlinked if the third loop is removed. In the figure, the role of one of these three loops is taken by the center of the spiral roll, which does not actually form a loop, so this embedding is not topologically linked. From the arrangement of the loops in the cutaway view it is possible to unlink it by pulling the right half of the red band to the right and up, around the right end of the yellow spiral center, passing this part of the red band around the right half of the blue band, and then passing the same part of the red band back to the right and down around the right end of the yellow spiral center. This sequence of motions reverses the front-back order of the two red-blue crossings on the right half of the red band, after which it is straightforward to flatten the whole surface. We have also verified that this configuration is topologically unlocked using a physical model of two rubber bands attached to a pen.

As a smoothly-embedded surface, Figure 6 is locked: it cannot be flattened while preserving its geometry. To prove this, we use three interlocked properties of the embedding that, like the Borromean rings, are interlinked: as long as any two of the properties remain valid, the third one must remain valid as well, so none of the three properties can be the first to break

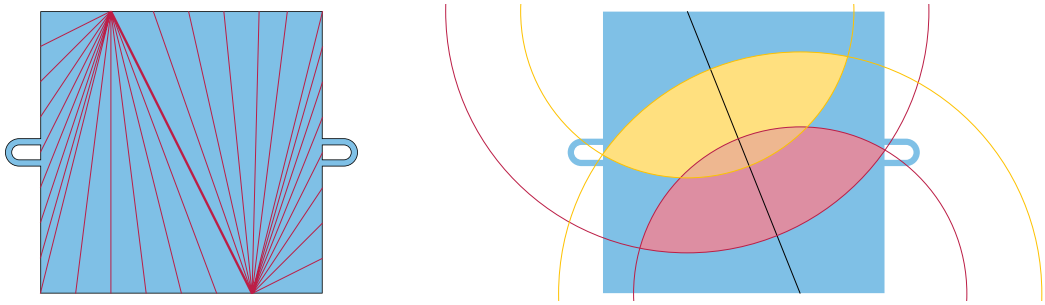

Figure 7 Left: Bend lines for a deformed version of Figure 6 in which the (heavier) bend line through the center of the square crosses the top and bottom sides of the square at distance 1/4 from the sides. Right: For a bend line through the square's center (shown at distance 3/10 from the sides), the attachment point of the right loop must be in the red shaded lune, the intersection of two circles (both centered at the bend endpoints and passing through the point where the loop is attached in the unrolled view of the square), to avoid having greater distance to those endpoints than in the flattened surface. Symmetrically, the attachment point of the left loop must be in the yellow shaded lune. These lunes overlap only near the center of the square, forcing the two entangled loops to be near that point. If the bend line were at distance 1/4 from the sides, the two lunes would touch but not overlap, and for a bend line even closer to the sides, the lunes would become disjoint, preventing the loops from being both near each other and having points of attachment within each lune.

in any continuous motion of the embedding. The first two properties are parameterized by a parameter ε, which we will be able to make arbitrarily small by making the length of the loops sufficiently small:

- ***A***. The two loops are bounded within distance ε of each other.
- ***B***. The nearest bend line on the square to its center point has distance $\leq \varepsilon$ to the center point, and crosses the top and bottom sides of the square at distance $\geq 1/4 - \varepsilon$ from its left and right sides.
- ***C***. The nearest bend line on the square to its center point can be completed into a loop by a curve, on a sphere with it as diameter, forming Borromean rings with the other two loops.

The reason for the 1/4 in property B is that it is possible to deform Figure 6, keeping the two loops interlocked in the center of the roll, so that the center bend line crosses the top and bottom sides of the square at distance 1/4, as shown in Figure 7(left). However, as we will prove, it is not possible to move this center bend line significantly farther from vertical.

▶ **Lemma 5** ($A \wedge B \Rightarrow C$). *For all sufficiently small loop lengths δ and all sufficiently small ε, continuous motion through states where $A(\varepsilon)$ and $B(\varepsilon)$ hold, starting from a state where C holds, cannot reach a state where C does not hold.*

Proof. Let b be the bend line of property B. Then (Figure 7, right) the attachment point p of the right loop must lie within the intersection of two spheres centered at the endpoints of b, with radii equal to the distances from p to those endpoints, because the embeddings we consider are not allowed to increase distances. Similarly, the attachment point of the left loop must lie within the intersection of another two spheres. By property A, these attachment points must be near each other, and until C stops holding, they must also lie near line b. This limits their nearby locations to points of line b that are far from its endpoints on the

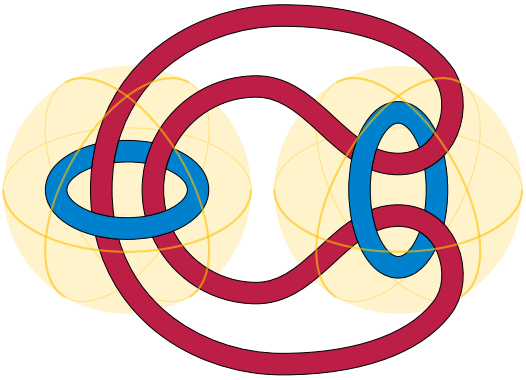

Figure 8 Borromean rings with links in separate spheres

square, so they cannot reach the sphere through the endpoints of b on which the connecting curve of property C lies.

As the smooth embedding deforms continuously, the bend line nearest the center point can change, but (as long as B continues to hold) only by small amounts, and the connecting curve can be changed by similar small amounts to maintain property C. As the other two loops cannot reach the sphere containing this curve, they cannot cross this curve (even though it does not form a physical obstacle to them) and cannot change the knotted topology that it forms with them. ◀

▶ **Lemma 6** ($A \wedge C \Rightarrow B$)**.** *For all sufficiently small ε there exists a δ such that, for loop lengths less than δ, continuous motion through states where $A(2\varepsilon)$ and C hold, starting from a state where $B(\varepsilon)$ holds, cannot reach a state where $B(\varepsilon)$ does not hold.*

Proof. Let b be the bend line nearest the center of the square. While A and C hold, b must pass through the Borromean link formed by it and the two loops, and so (if the center point itself does not lie on a bend line) it must lie on a flattened part of the surface whose width is at most proportional to the loop length. Therefore, b is close to the center point, as part of property B demands. For a bend line that is close to the center point, the same reasoning used in Figure 7 (right) and Lemma 5 shows that it must be at distance at least $1/4 - \varepsilon$ from the left and right sides, for otherwise the two intervals on this bend line where the left and right loop attachment points must be near would not intersect. ◀

▶ **Lemma 7** ($B \wedge C \Rightarrow A$)**.** *For all sufficiently small ε there exists a δ such that, for loop lengths less than δ, continuous motion through states where $B(2\varepsilon)$ and C hold, starting from a state where $A(\varepsilon)$ holds, cannot reach a state where $A(\varepsilon)$ does not hold.*

Proof. By assumption C, the two loops of the surface and a third loop formed by bend line b form Borromean rings, and by assumption B, line b is near vertical and near the square's center, forcing the attachment points of the two loops to be far from the endpoints of b.

Each loop of the surface has small diameter, so if the two loops could be far from each other it would be possible to make two small spheres (of radius ε), one containing each loop. The loop containing b lies on a straight line within each of these two spheres. Although Borromean rings can have two loops in two disjoint spheres [29], as depicted in Figure 8, the third Borromean ring cannot pass through either sphere as a straight line. If it could, we could deform a loop within its sphere to a circle (as it is not pairwise linked with the line passing through the sphere) and span it by a disk not crossed by the other two loops,

impossible for the Borromean rings. This contradiction shows that the two loops cannot be separated by a distance larger than ε, as stated in property A. ◀

These properties together prove that the surface of Figure 6 is locked: for versions of this surface with short enough loops, it is impossible to deform it as a smoothly embedded surface to its flattened state. The same is true for the same reasons for approximations to this surface by polyhedral embeddings or flat foldings without interior vertices. As a result, we have the following theorem:

▶ **Theorem 8.** *For smooth embeddings, polyhedral embeddings without interior vertices, and flat foldings without interior vertices, there exist flat surfaces with the topology of a disk with two holes that are ambient isotopic to their flattened form but cannot reach that form by a continuous sequence of folded states staying within the same class of folded states.*

Proof. Choose a sufficiently small $\delta > 0$ and $\varepsilon > 0$ for the lemmas above, and small enough that Lemma 5 remains valid for 2ε in place of ε. A surface in the configuration of Figure 6 can be constructed with loop lengths $\leq \delta$ and with properties $A(\varepsilon)$, $B(\varepsilon)$, and C, by rolling the surface with vertical bend lines within a radius small enough to allow loops of these lengths to wrap around it in that configuration. If this surface moves continuously, starting from this initial configuration, all three properties must remain true; none can be the first to fail (nor can two or three of these properties fail simultaneously). This is because, at the instant any one or more of these properties first failed, the weaker properties $A(2\varepsilon)$ and $B(2\varepsilon)$ would still be true. Thus, we would still have a continuous motion through configurations in which which $A(2\varepsilon)$ and $B(2\varepsilon)$ remain true throughout the motion, starting from a state where C is true. By Lemma 5, C must remain true at the end of such a motion. Then, by Lemma 6 and Lemma 7, $B(\varepsilon)$ and $A(\varepsilon)$ (respectively) must also remain true at the end of the motion, contradicting the assumption that it is possible for one or more of these properties to have failed. ◀

5 Conclusions and open problems

We have shown that, for smooth embeddings, polyhedral embeddings without interior vertices, and flat foldings without interior vertices, every spiral-shaped domain can be flattened. However, there exist more complex planar shapes whose configuration spaces are disconnected: they have locked embeddings that, although topologically equivalent, cannot be flattened.

Is every topological disk flattenable? Can the method that we used to flatten Figure 4 be generalized to other disks? What about surfaces with a single hole? Additionally, we have only investigated the existence of flattenings, but not their algorithmic complexity. For polyhedral embeddings and flat foldings, how hard is it to determine whether a continuous flattening exists? What about for smooth embeddings represented as a piecewise cylindrical and conical surface?

A Recognizing polygonal spiral-shaped domains

In this section we provide a linear-time algorithm for recognizing the polygons that have inward-spiraling shrinking motions. We defer this material to an appendix as it is somewhat tangential to our main results on reconfiguration of surfaces.

The *polar tangential angle* of a curve, at any point, is the angle between the curve and a ray from the origin through the point. The logarithmic spirals can be characterized as the

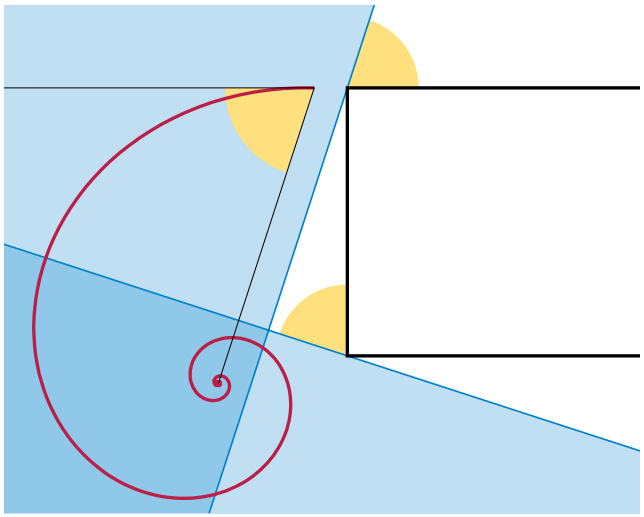

Figure 9 A counterclockwise inward-spiraling motion whose spirals (red) have polar tangential angle 72° (yellow), inside a polygon (thick black edges). According to Lemma 9, the center of the motion must lie in the intersection of the shaded blue halfplanes.

curves for which all points have the same polar tangential angle, and this angle completely determines the shape of the spiral. In an inward-spiraling shrinking motion, each point of the set S traces out a logarithmic spiral, whose polar tangential angle θ is determined by the motion: all points have the same angle and trace out spirals of the same shape. For the motion to be continuously shrinking, it must be the case that all of these logarithmic spirals remain entirely inside the given shape.

Although the general problem of finding inward-spiraling shrinking motions allows the polar tangential angle to vary, we begin by characterizing the existence of such a motion for a fixed choice of θ. As our next lemma shows, fixing θ significantly simplies this problem. It allows the problem to be solved in terms of the non-emptiness of an intersection of halfplanes (linear programming feasibility), much like the problem of recognizing star-shaped polygons.

▶ **Lemma 9.** *For a given simple polygon P, an inward-spiraling shrinking motion with a polar tangential angle θ and center c exists if and only if c lies within an intersection of halfplanes, passing through the vertices of P. For a counterclockwise spiraling motion, the halfplane through vertex v lies on a line rotated counterclockwise by angle θ from the edge of P that is counterclockwise from v, as shown in Figure 9. For a clockwise spiraling motion, symmetrically, the halfplane through vertex v lies on a line rotated clockwise by angle θ from the edge of P that is clockwise from v. As a special case, when $\theta = 0$, we get a halfplane bounded by each edge of the polygon, without rotation; it makes no difference which of the two vertices of the edge we associate to this halfplane.*

Proof. If $\theta = 0$, each halfplanes defines the region of the polygon within which its edge is visible, and their intersection is the standard construction of the kernel of a star-shaped polygon. Otherwise, we can assume that $\theta \neq 0$. Each edge e of P, is associated with one of the halfplanes of the lemma, passing through an endpoint v of e. If c is outside this halfplane, then lines from c to points of e near v will cross v at a shallower angle than θ. This implies that a spiral with polar tangential angle θ and center c, starting from a point of e sufficiently near v, will start in a direction that takes it out of P, so we do not have a valid inward-spiraling motion of P.

On the other hand, if c is inside the halfplane for edge e, all line segments from c to e will meet e at a wider angle than θ. This implies that all spirals that start from points of e with polar tangential angle θ and center c will start in a direction that enters P. If this is the case for all edges of P, then this motion initially takes the boundary of P to the interior of P. This motion must be a valid inward-spiraling motion for all points of P (not just its boundary points), and for all times until the polygon shrinks to the center of the motion (not just initially), because there is no point of the boundary at which the spiral traced by one of the points of P can cross back out of P. ◀

Based on standard properties of intersecting halfplanes, we have the following characterization of infeasible angles θ for the existence of an inward-spiraling shrinking motion.

▶ **Observation 10.** *Suppose that, for a given polygon P and angle θ, no inward-spiraling shrinking motion exists; that is, by Lemma 9, the halfplanes described by Lemma 9 have an empty intersection. Then either two of these halfplanes have parallel boundary lines and an empty intersection, or three of these halfplanes have pairwise non-parallel boundary lines and an empty intersection.*

Thus, to determine whether a polygon P has an inward-spiraling shrinking motion, we need only determine whether there exists an angle θ for which every pair or triple of the halfplanes of Lemma 9 has a non-empty intersection. We will consider the clockwise motions separately from the counterclockwise ones, so that as we vary θ each halfspace rotates around a single point (one of the endpoints of its defining polygon edge). As we will see, with this restriction, each pair or triple of halfplanes has only a single *critical angle*, separating the angles with empty intersection from the angles with non-empty intersection. The case of pairs of halfplanes is simplest:

▶ **Lemma 11.** *Let e and e' be two edges of polygon P with the same slope and opposite orientations. Then the halfplanes defined by e and e' have at most one critical angle for clockwise inward-spiraling shrinking motions, and at most one critical angle for counterclockwise inward-spiraling shrinking motions.*

Proof. Suppose that we are considering counterclockwise motions, as depicted in Figure 9; the case for clockwise motions is symmetric. For any polar tangential angle θ, the two halfplanes defined for e and e' in Lemma 9 will have parallel boundary lines, and will extend in opposite directions from their lines. If we vary θ continuously, the position of these two halfplanes will also vary continuously, rotating around the endpoints v and v' of e and e' respectively. Note that v and v' are necessarily distinct vertices of P. By continuity, an angle θ can be critical (separating angles with empty intersection from angles with nonempty intersection) when the boundary lines for the two halfplanes for angle θ coincide. This can only happen at the unique angle that causes these lines to pass through both v and v'. ◀

To prove a corresponding lemma about triples of non-parallel halfspaces, we need the following observation about how pairs of non-parallel halfspaces meet each other.

▶ **Observation 12.** *Let e and e' be two edges of polygon P with different slopes, forming an angle ϕ. Then, as θ varies (either for clockwise or counterclockwise motions), and as the halfplanes defined from e and e' rotate around their endpoints v and v', their two boundary lines maintain a constant angle ϕ, because both boundary lines are rotated by θ from e and e'. The intersection of the two boundary lines lies on a circle through v and v', the locus of points forming angle ϕ with v and v'.*

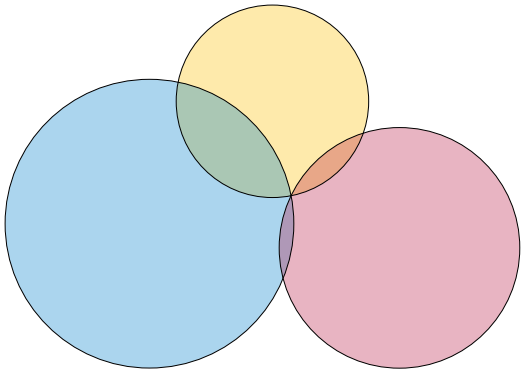

Figure 10 Three circles that cross pairwise at three distinct points can only have a single triple crossing.

Using this, we have:

▶ **Lemma 13.** *Let e, e', and e'' be three edges of polygon P with three different slopes. Then the halfplanes defined by e, e', and e'' have at most one critical angle for clockwise inward-spiraling shrinking motions, and at most one critical angle for counterclockwise inward-spiraling shrinking motions.*

Proof. By continuity, θ can only be a critical angle when the three halfplanes defined by e, e', and e'' with endpoints v, v', and v'' meet at a single point, which must be a point of intersection of the three circles defined by Observation 12 for pairs of these three halfplanes. However, two of these circles meet at each of the three points v, v', and v''. Because any two circles in the plane can only cross each other twice, and one of these two potential crossing points is already used up by the crossings at v, v', and v'', the three circles can only have one triple point (Figure 10). ◀

To recognize polygons with (clockwise or counterclockwise) inward-spiraling shrinking motions, we use the theory of *LP-type problems*. An LP-type problem can be defined by a function f from finite subsets of a given finite set S to a totally-ordered set, with the following properties:

- For every two sets A and B satisfying $A \subset B \subset S$, f is *monotonic*: $f(A) \leq f(B)$.
- For every two sets A and B satisfying $A \subset B \subset S$ and every element e of S, f is *local*: if $f(A) = f(B) = f(A \cup \{e\})$, then these three evaluations of f also equal $f(B \cup \{e\})$.

A set $B \subset S$ is a *basis* if no other subset $A \subset B$ has the same evaluation, and the *combinatorial dimension* of the problem is the maximum cardinality of a basis. The goal of an LP-type problem is to determine the value of $f(S)$ using only evaluations of f on small sets, of size related to the combinatorial dimension. When the dimension is $O(1)$, this can be done using $O(n)$ evaluations of f on sets of size $O(1)$.

The original algorithms for linear-time solution of LP-type problems, and the ones with the best time dependence on the dimension, are randomized [24]. However, for geometric optimization problems for which a *subsystem oracle* is available, it is possible to obtain a deterministic $O(n)$ time bound [7]. This subsystem oracle should take as input a subset A of elements of S, and list all subsets of A that can be obtained from any basis B of S as

$$\Big\{e \in A \mid f(B) \neq f\big(B \cup \{e\}\big)\Big\}.$$

It must do this in an amount of time that depends polynomially on A, even though the number of bases B of S used to define its output can be considerably larger. More precisely, in order to obtain a deterministic linear time algorithm, the number of output sets should be $O(|A|^D)$, and it should be possible to list them all in time $O(|A|^{D+1})$, for some number D known as the *shatter dimension* of the problem. Because of this required time bound, the subsystem oracle does not have time to consult S as input, and may produce a larger family of sets, ones that could be produced from a base of any problem of the same type rather than from the specific problem defined by S. Not all LP-type problems of bounded combinatorial dimension also have bounded shatter dimension and a fast subsystem oracle, but when the shatter dimension is bounded, and a subsystem oracle can be constructed for it, this is enough to lead to a deterministic linear time algorithm [7]. By the Sauer–Shelah lemma, bounding the shatter dimension is equivalent to bounding the *Vapnik–Chervonenkis* dimension of the same system of sets, defined as the largest input size m for which there exists an input to the subsystem oracle that causes it to return all 2^m subsets of its input [23, 25].

We now apply these concepts to our problem.

▶ **Lemma 14.** *Let S consist of the edges of a given polygon P, and let $\varphi(A)$ be the minimum angle θ for which the (closed) halfplanes defined by Lemma 9 for counterclockwise inward-spiraling shrinking motions, for the edges in A, have a non-empty intersection. Let $f(A)$ map A to the triple $(\varphi(A), x, y)$ where (x, y) is the lexicographically minimum point in this intersection, and order these triples lexicographically. Then f defines an LP-type problem of dimension at most 3.*

Proof. The range of angles $[0, \pi]$ possible for φ, and the (closed) polygon P within which the point (x, y) must lie both form compact sets, so by compactness f has a well-defined value. The function f defined in this way is clearly monotonic: adding more halfplanes can only eliminate some triples (φ, x, y) from being part of a non-empty intersection, and therefore can increase or leave unchanged the minimum triple at which the intersection is non-empty. It is local, because if a triple (φ, x, y) is the optimal triple for a non-empty intersection for A, B, and $A \cup \{e\}$, point (x, y) must belong to the halfplane defined for φ and e, and therefore the triple remains optimal when this halfplane is added to those for B.

It remains to prove that the dimension is at most 3. Therefore, let B be any basis of S; we must show that $|B| \leq 3$. Let $f(B) = (\varphi, x, y)$; then for every $\varphi' < \varphi$, some subset A of B with $|A| \leq 3$ has an empty intersection of halfplanes, by Observation 10. Since there are only finitely many choices of A, we can choose A so that it has an empty intersection for values of φ' arbitrarily close to φ; however, because (x, y) belongs to the intersection of all the halfspaces for B for angle φ, the halfplanes in A for angle φ also have nonempty intersection. Thus, φ is a critical angle for A. By Lemma 11 and Lemma 13, there can be only one critical angle, so in particular it is impossible for the halfspaces for A to have a non-empty intersection for any $\varphi' < \varphi$. Therefore, $f(A) = (\varphi, x', y')$ for some x' and y'. That is, A determines the optimal angle φ, although possibly not the optimal x and y for that angle.

Because A is critical at angle φ, its halfplanes intersect to form either a line (if $|A| = 2$) or a single point (if $|A| = 3$). In the $|A| = 3$ case, this point must be (x, y). In the $|A| = 2$ case, a single additional halfplane suffices to determine the lexicographically minimal point (x, y). Thus, in either case, the triple (φ, x, y) is determined by three elements of B. Since B was assumed to be a minimal subset determining this triple, $|B| = 3$. ◀

▶ **Lemma 15.** *There exists a subsystem oracle for the LP-type problem defined in Lemma 14, of shatter dimension ≤ 3.*

Proof. For a given set A, with $|A| = m$, each of the subsets $\{e \in A \mid f(B) \neq f(B \cup \{e\})\}$ that should be returned from the subsystem oracle can be determined from the triple (θ, x, y) with $\theta = \varphi(B)$ defined for B in Lemma 14. It is the subset of elements of A for which the rotated halfplane with angle θ does not contain the point (x, y).

For any fixed choice of θ there are $O(m^2)$ of these sets. They can be obtained by rotating a halfplane with angle θ for each element of A, drawing the arrangement of m lines bounding the rotated halfplanes, and constructing one set for each face of the resulting arrangement of lines, consisting of the halfplanes disjoint from that face. This arrangement of lines changes combinatorially at the angles θ for which three of the rotated halfplane boundaries meet at a point, which happens at $O(m^3)$ angles by Lemma 13. At these angles, one face of the arrangement shrinks to a point and a different face appears. Away from these critical angles, or in faces that do not appear or disappear at a critical angle, the subsets returned by the subsystem oracle do not change.

Therefore, there are $O(m^3)$ of these subsets altogether. They can be obtained in $O(m^4)$ time by constructing and sorting the critical angles for each triple of edges in the input set A, using the sorted sequence of critical angles to trace through the sequence of combinatorial changes to the arrangement of boundary lines of rotated halfplanes, and outputting for each newly formed arrangement face a list of the halfplanes that are disjoint from that face. ◀

▶ **Theorem 16.** *It is possible to determine whether a given polygon P has an inward-spiraling shrinking motion, and if so to determine a feasible center and polar tangential angle for such a motion, in time linear in the number of vertices of the polygon.*

Proof. We apply a deterministic linear-time bounded-dimension LP-type algorithm two times, once by Lemma 14 to determine whether it has a counterclockwise inward-spiraling shrinking motion, and a second time by a symmetric argument to determine whether it has a clockwise inward-spiraling shrinking motion. ◀

References

1. Zachary Abel, Jason Cantarella, Erik D. Demaine, David Eppstein, Thomas C. Hull, Jason S. Ku, Robert J. Lang, and Tomohiro Tachi. Rigid origami vertices: conditions and forcing sets. *Journal of Computational Geometry*, 7(1):171–184, 2016. doi:10.20382/jocg.v7i1a9.
2. Dov Aharonov, Mark Elin, and David Shoikhet. Spiral-like functions with respect to a boundary point. *Journal of Mathematical Analysis and Applications*, 280(1):17–29, 2003. doi:10.1016/S0022-247X(02)00615-7.
3. Brad Ballinger, David Charlton, Erik D. Demaine, Martin L. Demaine, John Iacono, Ching-Hao Liu, and Sheung-Hung Poon. Minimal locked trees. In Frank K. H. A. Dehne, Marina L. Gavrilova, Jörg-Rüdiger Sack, and Csaba D. Tóth, editors, *Algorithms and Data Structures, 11th International Symposium, WADS 2009, Banff, Canada, August 21-23, 2009. Proceedings*, volume 5664 of *Lecture Notes in Computer Science*, pages 61–73. Springer, 2009. doi:10.1007/978-3-642-03367-4_6.
4. Therese Biedl, Erik D. Demaine, Martin L. Demaine, Sylvain Lazard, Anna Lubiw, Joseph O'Rourke, Mark Overmars, Steve Robbins, Ileana Streinu, Godfried Toussaint, and Sue Whitesides. Locked and unlocked polygonal chains in three dimensions. *Discrete & Computational Geometry*, 26(3):269–281, 2001. doi:10.1007/s00454-001-0038-7.
5. Therese Biedl, Erik D. Demaine, Martin L. Demaine, Sylvain Lazard, Anna Lubiw, Joseph O'Rourke, Steve Robbins, Ileana Streinu, Godfried Toussaint, and Sue Whitesides. A note on reconfiguring tree linkages: trees can lock. *Discrete Applied Mathematics*, 117(1-3):293–297, 2002. doi:10.1016/S0166-218X(01)00229-3.
6. Therese Biedl, Anna Lubiw, and Julie Sun. When can a net fold to a polyhedron? *Computational Geometry*, 31(3):207–218, 2005. doi:10.1016/j.comgeo.2004.12.004.

7 Bernard Chazelle and Jiří Matoušek. On linear-time deterministic algorithms for optimization problems in fixed dimension. *Journal of Algorithms*, 21(3):579–597, 1996. doi:10.1006/jagm.1996.0060.

8 Robert Connelly, Erik D. Demaine, Martin L. Demaine, Sándor P. Fekete, Stefan Langerman, Joseph S. B. Mitchell, Ares Ribó, and Günter Rote. Locked and unlocked chains of planar shapes. *Discrete & Computational Geometry*, 44(2):439–462, 2010. doi:10.1007/s00454-010-9262-3.

9 Robert Connelly, Erik D. Demaine, and Günter Rote. Straightening polygonal arcs and convexifying polygonal cycles. *Discrete & Computational Geometry*, 30(2):205–239, 2003. doi:10.1007/s00454-003-0006-7.

10 Erik D. Demaine, Martin L. Demaine, Vi Hart, John Iacono, Stefan Langerman, and Joseph O'Rourke. Continuous blooming of convex polyhedra. *Graphs and Combinatorics*, 27(3):363–376, 2011. doi:10.1007/s00373-011-1024-3.

11 Erik D. Demaine, Satyan L. Devadoss, Joseph S. B. Mitchell, and Joseph O'Rourke. Continuous foldability of polygonal paper. In *Proceedings of the 16th Canadian Conference on Computational Geometry, CCCG'04, Concordia University, Montréal, Québec, Canada, August 9-11, 2004*, pages 64–67, 2004. URL: https://www.cccg.ca/proceedings/2004/55.pdf.

12 Erik D. Demaine, Stefan Langerman, Joseph O'Rourke, and Jack Snoeyink. Interlocked open and closed linkages with few joints. *Computational Geometry*, 26(1):37–45, 2003. doi:10.1016/S0925-7721(02)00171-2.

13 Erik D. Demaine and Joseph S. B. Mitchell. Reaching folded states of a rectangular piece of paper. In *Proceedings of the 13th Canadian Conference on Computational Geometry, University of Waterloo, Ontario, Canada, August 13-15, 2001*, pages 73–75, 2001. URL: https://erikdemaine.org/papers/PaperReachability_CCCG2001/.

14 David Eppstein. Realization and connectivity of the graphs of origami flat foldings. *Journal of Computational Geometry*, 10(1):257–280, 2019. doi:10.20382/jocg.v10i1a10.

15 Dmitry Fuchs and Serge Tabachnikov. Lecture 14: Paper Möbius band. In *Mathematical Omnibus: Thirty Lectures on Classic Mathematics*, pages 199–206. American Mathematical Society, Providence, Rhode Island, 2007. doi:10.1090/mbk/046.

16 Yue Hao, Yun hyeong Kim, and Jyh-Ming Lien. Synthesis of fast and collision-free folding of polyhedral nets. In *Proceedings of the 2nd ACM Symposium on Computational Fabrication*, June 2018. doi:10.1145/3213512.3213517.

17 Denis F. Hinz and Eliot Fried. Translation of Michael Sadowsky's paper "An elementary proof for the existence of a developable Möbius band and the attribution of the geometric problem to a variational problem". *Journal of Elasticity*, 119(1-2):3–6, 2015. doi:10.1007/s10659-014-9490-5.

18 John Hopcroft, Deborah Joseph, and Sue Whitesides. Movement problems for 2-dimensional linkages. *SIAM Journal on Computing*, 13(3):610–629, 1984. doi:10.1137/0213038.

19 D. T. Lee and F. P. Preparata. An optimal algorithm for finding the kernel of a polygon. *Journal of the ACM*, 26(3):415–421, 1979. doi:10.1145/322139.322142.

20 Ezra Miller and Igor Pak. Metric combinatorics of convex polyhedra: Cut loci and nonoverlapping unfoldings. *Discrete & Computational Geometry*, 39(1-3):339–388, 2008. doi:10.1007/s00454-008-9052-3.

21 Gaiane Panina and Ileana Streinu. Flattening single-vertex origami: The non-expansive case. *Computational Geometry*, 43(8):678–687, 2010. arXiv:1003.3490, doi:10.1016/j.comgeo.2010.04.002.

22 John Pardon. On the unfolding of simple closed curves. *Transactions of the American Mathematical Society*, 361(4):1749–1764, 2009. doi:10.1090/S0002-9947-08-04781-8.

23 N. Sauer. On the density of families of sets. *J. Combinatorial Theory, Ser. A*, 13:145–147, 1972. doi:10.1016/0097-3165(72)90019-2.

24 Micha Sharir and Emo Welzl. A combinatorial bound for linear programming and related problems. In *Proceedings of the 9th Annual Symposium on Theoretical Aspects of Computer*

Science (STACS 1992), volume 577 of *Lecture Notes in Computer Science*, pages 567–579. Springer-Verlag, 1992. doi:10.1007/3-540-55210-3_213.

25 Saharon Shelah. A combinatorial problem; stability and order for models and theories in infinitary languages. *Pacific J. Math.*, 41:247–261, 1972. doi:10.2140/pjm.1972.41.247.

26 Guang Song and Nancy M. Amato. A motion-planning approach to folding: From paper craft to protein folding. *IEEE Transactions on Robotics and Automation*, 20(1):60–71, February 2004. doi:10.1109/tra.2003.820926.

27 Ileana Streinu. A combinatorial approach to planar non-colliding robot arm motion planning. In *Proceedings of the 41st IEEE Symposium on Foundations of Computer Science*, pages 443–453, 2000. doi:10.1109/SFCS.2000.892132.

28 Ileana Streinu and Walter Whiteley. Single-vertex origami and spherical expansive motions. In *Discrete and Computational Geometry: Japanese Conference, JCDCG 2004, Tokyo, Japan, October 8-11, 2004, Revised Selected Papers*, volume 3742 of *Lecture Notes in Computer Science*, pages 161–173. Springer-Verlag, 2005. doi:10.1007/11589440_17.

29 Morwen B. Thistlethwaite. On the algebraic part of an alternating link. *Pacific Journal of Mathematics*, 151(2):317–333, 1991. doi:10.2140/pjm.1991.151.317.

30 Nicholas Turner, Bill Goodwine, and Mihir Sen. A review of origami applications in mechanical engineering. *Proceedings of the Institution of Mechanical Engineers, Part C*, 230(14):2345–2362, August 2015. doi:10.1177/0954406215597713.

31 Zhonghua Xi and Jyh-Ming Lien. Continuous unfolding of polyhedra – a motion planning approach. In *Proceedings of the 2015 IEEE/RSJ International Conference on Intelligent Robots and Systems (IROS)*. IEEE, September 2015. doi:10.1109/iros.2015.7353828.